Resource

Cell Reports

Calcium Transient Dynamics of Neural Ensembles in the Primary Motor Cortex of Naturally Behaving Monkeys

Graphical Abstract

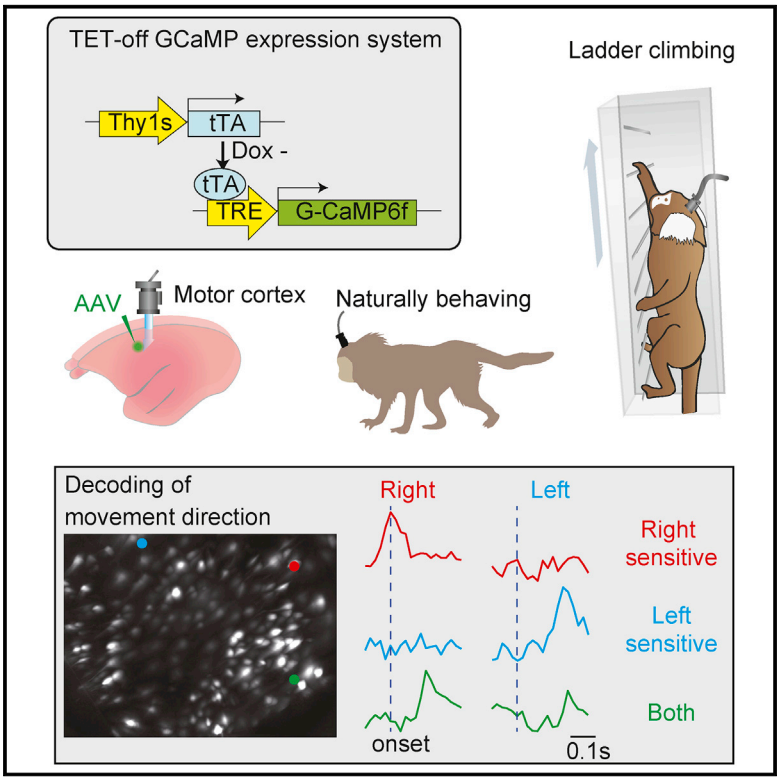

Highlights

- Ca^{2+} imaging with a miniature microscope demonstrated in marmoset motor cortex
- Neuronal populations during naturalistic behavior recorded
- The technology allows study of human-relevant behavior such as social interactions

Authors

Takahiro Kondo, Risa Saito, Masaki Otaka, ..., Kenji F. Tanaka, Junichi Ushiba, Hideyuki Okano

Correspondence

ushiba@brain.bio.keio.ac.jp (J.U.), hidokano@a2.keio.jp (H.O.)

In Brief

Kondo et al. demonstrate calcium imaging from neuronal populations using a miniature fluorescence microscope in naturally behaving non-human primates (NHPs), common marmosets. This technique marks an advance beyond methods that use fixed head positioning, which limits the study of complex, self-determined behaviors such as social interactions or fear and anxiety.

Kondo et al., 2018, Cell Reports *24*, 2191–2195
August 21, 2018
https://doi.org/10.1016/j.celrep.2018.07.057

CellPress

Cell Reports
Resource

Calcium Transient Dynamics of Neural Ensembles in the Primary Motor Cortex of Naturally Behaving Monkeys

Takahiro Kondo,[1,2,14] Risa Saito,[3,14] Masaki Otaka,[3,14] Kimika Yoshino-Saito,[1,4] Akihiro Yamanaka,[5] Tetsuo Yamamori,[6] Akiya Watakabe,[6] Hiroaki Mizukami,[7] Mark J. Schnitzer,[8,9,10] Kenji F. Tanaka,[2,11] Junichi Ushiba,[12,13,*] and Hideyuki Okano[1,2,15,*]

[1]Department of Physiology, Keio University School of Medicine, Tokyo, Japan
[2]Laboratory for Marmoset Neural Architecture, RIKEN Center for Brain Science, Saitama, Japan
[3]Graduate School of Science and Technology, Keio University, Kanagawa, Japan
[4]Japan Society for the Promotion of Science, Tokyo, Japan
[5]Research Institute of Environmental Medicine, Nagoya University, Nagoya, Japan
[6]Laboratory for Molecular Analysis of Higher Brain Function, RIKEN Center for Brain Science, Saitama, Japan
[7]Division of Genetic Therapeutics, Center for Molecular Medicine, Jichi Medical University, Tochigi, Japan
[8]James H. Clark Center for Biomedical Engineering and Sciences, Stanford University, Stanford, CA, USA
[9]CNC Program, Stanford University, Stanford, CA, USA
[10]Howard Hughes Medical Institute, Stanford University, Stanford, CA, USA
[11]Department of Neuropsychiatry, Keio University School of Medicine, Tokyo, Japan
[12]Department of Biosciences and Informatics, Faculty of Science and Technology, Keio University, Kanagawa, Japan
[13]Keio Institute of Pure and Applied Sciences (KiPAS), Kanagawa, Japan
[14]These authors contributed equally
[15]Lead Contact
*Correspondence: ushiba@brain.bio.keio.ac.jp (J.U.), hidokano@a2.keio.jp (H.O.)
https://doi.org/10.1016/j.celrep.2018.07.057

SUMMARY

To understand brain circuits of cognitive behaviors under natural conditions, we developed techniques for imaging neuronal activities from large neuronal populations in the deep layer cortex of the naturally behaving common marmoset. Animals retrieved food pellets or climbed ladders as a miniature fluorescence microscope monitored hundreds of calcium indicator-expressing cortical neurons in the right primary motor cortex. This technique, which can be adapted to other brain regions, can deepen our understanding of brain circuits by facilitating longitudinal population analyses of neuronal representation associated with cognitive naturalistic behaviors and their pathophysiological processes.

INTRODUCTION

There is considerable interest in non-human primates (NHPs) as a neuroscientific model. NHPs can be used to study the neural circuits underlying social, cognitive, and motor behaviors that are highly relevant to humans. Two-photon microscopy, in combination with fluorescent, genetically encoded calcium indicators, has allowed the visualization of subcellular, single cellular, and ensemble neural dynamics and has become feasible in head-fixed monkeys (Nauhaus et al., 2012; Sadakane et al., 2015a; Seidemann et al., 2016; Yamada et al., 2016; Li et al., 2017; Ebina et al., 2018). However, complex behavior such as social interaction cannot be properly investigated using head fixation protocols. Furthermore, neural activities may differentially correlate with behaviors under head-fixed conditions compared to more natural conditions (Ziv and Ghosh, 2015). Miniaturized microscopes, in conjunction with an implantable microendoscopic lens, have enabled optical access to deep-brain neural ensembles in freely moving rodents (Ghosh et al., 2011). Here, we combined an optimized system for adeno-associated virus (AAV) vector expression of GCaMP with the appropriate microendoscope probe in the common marmoset (*Callithrix jacchus*). Thus, we demonstrate endoscopic miniature microscope imaging of multi-neuronal calcium transients in behaving NHPs.

RESULTS

To monitor task-related neural activity of primary motor cortex (M1) neurons, we first identified the left M1 via intracortical microstimulation (Figures 1A and S1A–S1C). Then, we injected AAVs expressing the Ca^{2+} indicator GCaMP6f (Chen et al., 2013) into the deep neocortical layers of the arm movement-related region (Figures S1C–S1H). We took advantage of the tetracycline-controlled transcriptional activation (Tet) system, an enhanced gene induction strategy, to sufficiently induce GCaMP6f and subsequently visualize transfected cells using an endoscope (Figures 1B and S2A). Furthermore, we optimized GCaMP6f levels by doxycycline (DOX) administration (Figures S2B and S2C).

We developed a monitoring system to track Ca^{2+} levels in 80–240 cells in a single field of view in individual marmosets (male, n = 3) (Figure 1C). We tested the system capability during naturalistic behavior in the marmosets, who engaged in a lever-pulling task while sitting (Figure 1D), and observed the activity of individual neurons during the task (Figure 1E). We

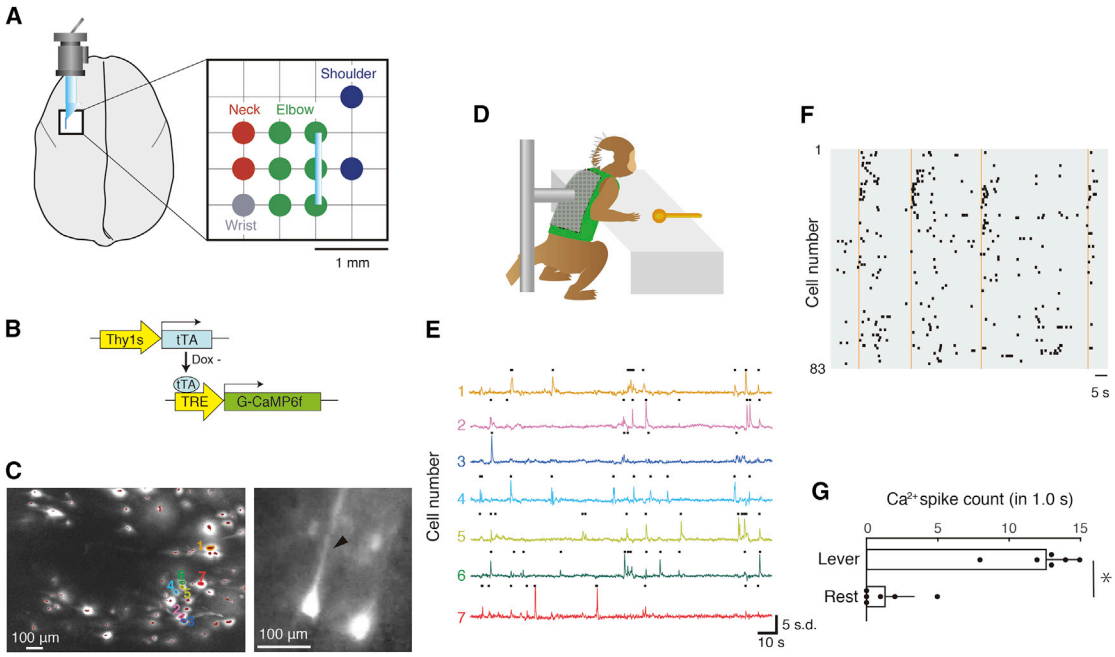

Figure 1. Recording of Movement-Related Ca^{2+} Transients from M1 Neurons

(A) Schematic of the calcium imaging setup. A craniotomy of 6 × 4 mm (3–9 mm anterior and 3–7 mm lateral relative to bregma) was performed over the left hemisphere. The microendoscopic lens (nVISTA; Inscopix, Palo Alto, CA) was implanted at the elbow area of M1, which was identified previously via intracortical microstimulation (ICMS; shown as the vertical blue line).

(B) Schematic of the GCaMP6f-based calcium indicator with the tetracycline-controlled transcriptional activation (Tet)-Off gene expression system. Tetracycline (tTA) activates the tetracycline response element (TRE3) promoter to amplify GCaMP6f expression. Doxycycline (DOX) inhibits the binding of tTA to the TRE3 promoter.

(C) Images of neurons in a single field of view with their region of interest (ROI) spatial filters. Each ROI spatial filter corresponds to a different independent component. Time traces for 7 of these cells (highlighted with brightly colored outlines in C) are shown in (E).

(D) Each marmoset wore a custom-made jacket with a Velcro strip that enabled experimenters to attach the marmoset's jacket to a back plate with a rigid bar.

(E) Relative changes in GCaMP6f fluorescence from a subset of individual neurons in (C). Black dots indicate detected Ca^{2+} events.

(F) Raster plot of the Ca^{2+} events. The vertical lines indicate the onset of lever pulling. The event frequency of the Ca^{2+} events increased with movement.

(G) Mean and SD of Ca^{2+} event count significantly increased during lever pulling in 1 s (from 83 neurons across 6 trials; t test, $p < 0.05$). The dots represent individual data. The error bars denote SD.

computationally extracted (Mukamel et al., 2009) the Ca^{2+} dynamics of individual cells from the imaging data and detected the Ca^{2+} events (Figures 1E and S3). We found that a subset of neurons was selectively active at the time during which the right forearm reached for the lever; other neurons were occasionally active during the rest period (Figure 1F). Overall, we found an increased incidence of Ca^{2+} events (12.5 ± 2.4, mean ± SD) during the lever-pulling task (Figures 1F and 1G). We next tested different and more naturalistic behaviors. To adapt to three-dimensional, rapidly moving marmosets with easily tangled microscope wire, we subjected the animals to a ladder-climbing task and found a movement-related increase in Ca^{2+} event incidence (Figure S4; Video S1).

What do these M1 neuronal activities encode during naturalistic voluntary arm movement? To address this question, the marmosets performed a seated bi-directional arm-reaching task (Figure 2A). We then employed a computational two-class discriminator to the neuronal Ca^{2+} data to decode the arm movement directions (STAR Methods). In this task, movement-direction-sensitive Ca^{2+} exciting neurons were observed during reaching (Video S2). We used partial least-squares discriminant analysis (PLS-DA) (Wold et al., 1984) to identify the neurons involved and the times at which information regarding movement direction occurred. The reaching movement sequences were segmented into three periods: before reaching onset (PRE-M), during reaching movement (MOV), and reaching offset (POST-M) (Figure 2B). Ca^{2+} excitation was detected in the MOV phase, as well as in the absence of arm movement during the PRE-M and POST-M periods (Figure 2C). PLS-DA, applied to the Ca^{2+} data acquired during each of the three periods, was able to accurately decode the reaching direction (marmoset M: PRE-M, 83.2% ± 5.4%; MOV, 90.1% ± 3.4%; POST-M, 82.1% ± 7.4%; mean ± SD) (Figure 2D).

The weight vector $a_{m,t}$ in the PLS-DA model, representing the extent of Ca^{2+} data contribution in decoding at the mth neuron and the tth frame, was normalized to a Z score; neurons with a Z score > 3 (upper 10th percentile during MOV in marmoset M) were defined as movement-direction-sensitive neurons. The number of movement-direction-sensitive neurons detected was 7 in PRE-M (3.42% of identified neurons), 20 in MOV (9.76%), and 8 in POST-M (3.90%) in marmoset M (see Table S1 for marmosets W and S). These neurons showed

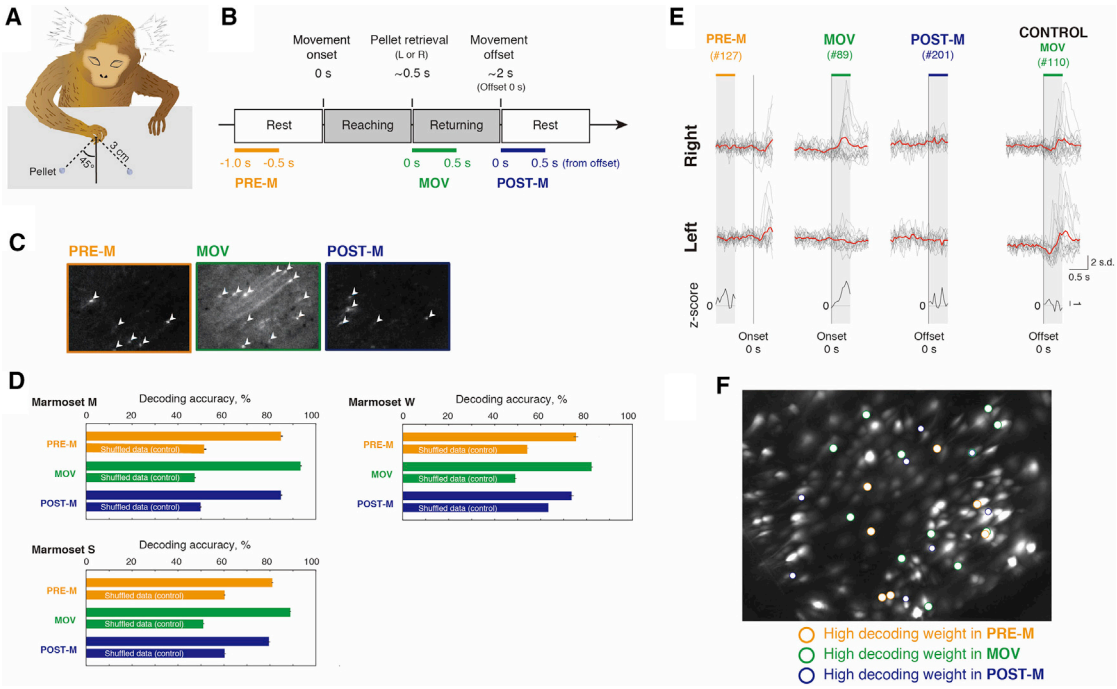

Figure 2. Decoding of Movement Direction from the Neuronal Ca^{2+} Transients of M1

(A) Pellet-reaching task. The pellet was placed 3 cm in front of and 45° to the right or left of the home position.

(B) Schematic of the task sequence and the period used for neural decoding. A marmoset sat in a chair and volitionally retrieved pellets by reaching one arm. The sequence of the reaching movement consisted of four periods: resting for a second, reaching one arm to the pellet, pulling back the arm holding the pellet, eating the pellet, and taking a rest. Ca^{2+} transient signals from −1.0 to −0.5 s from movement onset were segmented (PRE-M) and used for decoding of the neural signal movement planning. Ca^{2+} transient signals from the retrieval onset to 0.5 s after onset were segmented (MOV) and used for decoding of the neural signal movement execution. Ca^{2+} transient signals from the reaching offset to 0.5 s after offset were segmented (POST-M) and used for decoding of the neural signal motor trace.

(C) Examples of calcium imaging in the PRE-M, MOV, and POST-M periods. GCaMP fluorescence changes (arrowheads) were observed in all periods.

(D) Decoding accuracy of movement-direction estimation. Ca^{2+} transient signals from 200 isolated neurons in marmoset M, 120 neurons in marmoset S, and 241 neurons in marmoset W with respect to the PRE-M, MOV, and POST-M periods and the arm-reaching movement direction (either left or right) was predicted by partial least-squares discriminant analysis (PLS-DA). Not only Ca^{2+} events but also all Ca^{2+} transient signals were used for neural decoding (STAR Methods). As a control, the movement-direction labels were shuffled and the decoding accuracy was re-calculated, resulting in 50% (chance level). This suggests that the PLS decoder used in this study worked properly. The error bars denote SD.

(E) Representative Ca^{2+} transient signals of neurons contributing to movement-direction decoding. Neuron 127 showed movement-direction-sensitive Ca^{2+} transient in the PRE-M. The *Z* score assessed signal discrepancy. Similarly, neuron 89 showed movement-direction-sensitive Ca^{2+} transient in the MOV. Neuron 201 showed movement-direction-sensitive Ca^{2+} transient in the POST-M. However, neuron 110 showed Ca^{2+} transients to both right and left directional movements, and these waveforms were equivalent. No contribution to decoding was made in this case.

(F) Location of movement-direction-sensitive neurons. The results suggest that movement-direction-sensitive neurons in the POST-M did not participate in neural decoding during the PRE-M and MOV. Neurons contributing to neural decoding in PRE-M, MOV, and POST-M were randomly located, without significant spatial characteristics.

time- and phase-locked Ca^{2+} transients below the event detection threshold (Figure 2E). None of the other 170 neurons exhibited directional responses (e.g., neuron 110). Decoding using only these movement-direction-sensitive neurons kept high accuracy (e.g., marmoset M: PRE-M, 92.3% ± 11.9%; MOV, 90.7% ± 9.0%; POST-M, 80.0% ± 12.5%; mean ± SD).

In Figure 2F, we show the anatomical distribution of movement-direction-sensitive neurons. Neurons contributed to neural decoding in specific periods only (Table S1) and were randomly distributed anatomically. This suggests that movement-direction-sensitive neurons in POST-M did not participate in neural decoding during PRE-M and MOV (Figure S5), and the movement-direction-sensitive neurons in PRE-M and MOV did not contribute to neural decoding in POST-M (Table S1).

DISCUSSION

We developed a technique for endoscopic miniature microscope imaging in behaving NHPs, common marmosets, and monitored motor-related Ca^{2+} transient dynamics of M1 during several motor tasks. Using a longer gradient refractive index (GRIN) lens, the imaging method established in the present study is compatible with studies in imaging deeper brain areas. In addition, we developed the marmoset ladder apparatus to test a more naturalistic behavior with rapidly, freely moving marmosets. This apparatus may be expanded to other semi-open field behavioral procedures, such as the maze task and treadmill task (Foster et al., 2014). We also monitored motor-related Ca^{2+} transient dynamics of M1 during the bi-directional arm-reaching task. To

date, electrophysiological and fMRI studies indicate that M1 encodes information not only in motor planning and execution (Shenoy et al., 2013) but also in post-processing of movement (Hadipour-Niktarash et al., 2007; Orban de Xivry et al., 2011; Inoue et al., 2016). In a two-photon calcium imaging study in rodents, M1 individual neurons exhibited heterogeneous correlations with movement during even a simple lever-pull task (Peters et al., 2017). In the present study, the bi-directional arm-reaching task showed that M1 individual neurons exhibited heterogeneous activity, and we observed reaching movement-direction-sensitive neurons that were active in the POST-M but rarely recruited in the PRE-M or MOV. Further insights about the functional organization of motor cortex during reaching would be gained by using this technique.

This technology will make it possible to dissect large-scale neural circuits during human-relevant behavior under natural conditions, enabling the study of complex behaviors, including social interaction (Miller et al., 2016), fear, and anxiety (Barros and Tomaz, 2002; Shiba et al., 2017), and cognitive motor tasks. Furthermore, the relatively large marmoset brain will enable implantation of a pair of GRIN lenses near brain regions to monitor two interconnected areas, for example, M1 and the striatum, without using a complex, specially customized microscope (Lecoq et al., 2014). Consequently, the combination of this technique with transgenic marmoset technologies has the potential to transform our understanding, diagnosis, and treatment of human brain diseases (Izpisua Belmonte et al., 2015; Okano et al., 2016).

STAR★METHODS

Detailed methods are provided in the online version of this paper and include the following:

- KEY RESOURCES TABLE
- CONTACT FOR REAGENT AND RESOURCE SHARING
- EXPERIMENTAL MODEL AND SUBJECT DETAILS
- METHOD DETAILS
  - Intracortical microstimulation (ICMS) and adeno-associated virus (AAV) injection
  - Lens probe insertion and fixation
  - AAV production and purification
  - Doxycycline (DOX) treatment
  - Ladder-climbing task
  - Lever-pull and pellet retrieval tasks
  - Data processing
- QUANTIFICATION AND STATISTICAL ANALYSIS
  - Detection of spike events from Ca^{2+} transients
  - Partial least-squares discriminant analysis (PLS-DA)
  - Decoding arm-reaching movement direction using PLS-DA
  - Neural order shuffling

SUPPLEMENTAL INFORMATION

Supplemental Information includes five figures, one table, and two videos and can be found with this article online at https://doi.org/10.1016/j.celrep.2018.07.057.

ACKNOWLEDGMENTS

We thank Osamu Sadakane, Haruhiko Bito, Makoto Fukushima, Norio Takata, and the Inscopix member for technical support. This work was supported by a Grant-in-Aid for Young Scientists (B) (JP17K13067), and the Brain/MINDS project of the AMED (JP17dm0207002 and JP17dm0207001).

AUTHOR CONTRIBUTIONS

Conceptualization, T.K., K.F.T., M.J.S., J.U., and H.O.; Methodology, T.K., R.S., M.O., K.Y.-S., K.F.T., J.U., and H.O.; Software, R.S., M.O., and J.U.; Validation, T.K., K.F.T., J.U., and H.O.; Formal Analysis, R.S., M.O., J.U., and H.O.; Investigation, T.K., R.S., M.O., K.Y.-S., K.F.T., J.U., and H.O.; Resources, T.K., R.S., M.O., A.Y., T.Y., A.W., H.M., K.F.T., and H.O.; Data Curation, R.S., M.O., and J.U.; Writing – Original Draft, T.K., R.S., and J.U.; Writing – Review & Editing, M.J.S., K.F.T., J.U., and H.O.; Visualization, R.S., M.O., and J.U.; Supervision, M.J.S., K.F.T., J.U., and H.O.; Project Administration, K.F.T., J.U., and H.O.; Funding Acquisition, H.O.

DECLARATION OF INTERESTS

J.U. is a co-founder of Connect and jointly working with Panasonic. H.O. is a paid scientific advisory board member of San Bio and K Pharma. M.J.S. is a co-founder of and scientific consultant for Inscopix, which produced the miniature microscope.

Received: January 2, 2018
Revised: April 5, 2018
Accepted: July 16, 2018
Published: August 21, 2018

REFERENCES

Barros, M., and Tomaz, C. (2002). Non-human primate models for investigating fear and anxiety. Neurosci. Biobehav. Rev. *26*, 187–201.

Berger, T., Borgdorff, A., Crochet, S., Neubauer, F.B., Lefort, S., Fauvet, B., Ferezou, I., Carleton, A., Lüscher, H.-R., and Petersen, C.C.H. (2007). Combined voltage and calcium epifluorescence imaging *in vitro* and *in vivo* reveals subthreshold and suprathreshold dynamics of mouse barrel cortex. J. Neurophysiol. *97*, 3751–3762.

Chen, T.W., Wardill, T.J., Sun, Y., Pulver, S.R., Renninger, S.L., Baohan, A., Schreiter, E.R., Kerr, R.A., Orger, M.B., Jayaraman, V., et al. (2013). Ultrasensitive fluorescent proteins for imaging neuronal activity. Nature *499*, 295–300.

Ebina, T., Masamizu, Y., Tanaka, Y.R., Watakabe, A., Hirakawa, R., Hirayama, Y., Hira, R., Terada, S.-I., Koketsu, D., Hikosaka, K., et al. (2018). Two-photon imaging of neuronal activity in motor cortex of marmosets during upper-limb movement tasks. Nat. Commun. *9*, 1879.

Foster, J.D., Nuyujukian, P., Freifeld, O., Gao, H., Walker, R., Ryu, S.I., Meng, T.H., Murmann, B., Black, M.J., and Shenoy, K.V. (2014). A freely-moving monkey treadmill model. J. Neural Eng. *11*, 046020.

Ghosh, K.K., Burns, L.D., Cocker, E.D., Nimmerjahn, A., Ziv, Y., Gamal, A.E., and Schnitzer, M.J. (2011). Miniaturized integration of a fluorescence microscope. Nat. Methods *8*, 871–878.

Hadipour-Niktarash, A., Lee, C.K., Desmond, J.E., and Shadmehr, R. (2007). Impairment of retention but not acquisition of a visuomotor skill through time-dependent disruption of primary motor cortex. J. Neurosci. *27*, 13413–13419.

Inoue, M., Uchimura, M., and Kitazawa, S. (2016). Error signals in motor cortices drive adaptation in reaching. Neuron *90*, 1114–1126.

Izpisua Belmonte, J.C., Callaway, E.M., Caddick, S.J., Churchland, P., Feng, G., Homanics, G.E., Lee, K.-F., Leopold, D.A., Miller, C.T., Mitchell, J.F., et al. (2015). Brains, genes, and primates. Neuron *86*, 617–631.

Kondo, T., Yoshihara, Y., Yoshino-Saito, K., Sekiguchi, T., Kosugi, A., Miyazaki, Y., Nishimura, Y., Okano, H.J., Nakamura, M., Okano, H., et al. (2015).

Histological and electrophysiological analysis of the corticospinal pathway to forelimb motoneurons in common marmosets. Neurosci. Res. *98*, 35–44.

Konishi, M., Kawamoto, K., Izumikawa, M., Kuriyama, H., and Yamashita, T. (2008). Gene transfer into guinea pig cochlea using adeno-associated virus vectors. J. Gene Med. *10*, 610–618.

Lecoq, J., Savall, J., Vučinić, D., Grewe, B.F., Kim, H., Li, J.Z., Kitch, L.J., and Schnitzer, M.J. (2014). Visualizing mammalian brain area interactions by dual-axis two-photon calcium imaging. Nat. Neurosci. *17*, 1825–1829.

Li, M., Liu, F., Jiang, H., Lee, T.S., and Tang, S. (2017). Long-term two-photon imaging in awake macaque monkey. Neuron *93*, 1049–1057.e3.

Miller, C.T., Freiwald, W.A., Leopold, D.A., Mitchell, J.F., Silva, A.C., and Wang, X. (2016). Marmosets: a neuroscientific model of human social behavior. Neuron *90*, 219–233.

Mukamel, E.A., Nimmerjahn, A., and Schnitzer, M.J. (2009). Automated analysis of cellular signals from large-scale calcium imaging data. Neuron *63*, 747–760.

Nauhaus, I., Nielsen, K.J., Disney, A.A., and Callaway, E.M. (2012). Orthogonal micro-organization of orientation and spatial frequency in primate primary visual cortex. Nat. Neurosci. *15*, 1683–1690.

Okano, H., Sasaki, E., Yamamori, T., Iriki, A., Shimogori, T., Yamaguchi, Y., Kasai, K., and Miyawaki, A. (2016). Brain/MINDS: A Japanese national brain project for marmoset neuroscience. Neuron *92*, 582–590.

Orban de Xivry, J.J., Criscimagna-Hemminger, S.E., and Shadmehr, R. (2011). Contributions of the motor cortex to adaptive control of reaching depend on the perturbation schedule. Cereb. Cortex *21*, 1475–1484.

Pérez-Enciso, M., and Tenenhaus, M. (2003). Prediction of clinical outcome with microarray data: a partial least squares discriminant analysis (PLS-DA) approach. Hum. Genet. *112*, 581–592.

Peters, A.J., Lee, J., Hedrick, N.G., O'Neil, K., and Komiyama, T. (2017). Reorganization of corticospinal output during motor learning. Nat. Neurosci. *20*, 1133–1141.

Sadakane, O., Masamizu, Y., Watakabe, A., Terada, S., Ohtsuka, M., Takaji, M., Mizukami, H., Ozawa, K., Kawasaki, H., Matsuzaki, M., and Yamamori, T. (2015a). Long-term two-photon calcium imaging of neuronal populations with subcellular resolution in adult non-human primates. Cell Rep. *13*, 1989–1999.

Sadakane, O., Watakabe, A., Ohtsuka, M., Takaji, M., Sasaki, T., Kasai, M., Isa, T., Kato, G., Nabekura, J., Mizukami, H., et al. (2015b). In vivo two-photon imaging of dendritic spines in marmoset neocortex. eNeuro *2*, ENEURO.0019-15.2015.

Seidemann, E., Chen, Y., Bai, Y., Chen, S.C., Mehta, P., Kajs, B.L., Geisler, W.S., and Zemelman, B.V. (2016). Calcium imaging with genetically encoded indicators in behaving primates. eLife *5*, e16178.

Shenoy, K.V., Sahani, M., and Churchland, M.M. (2013). Cortical control of arm movements: a dynamical systems perspective. Annu. Rev. Neurosci. *36*, 337–359.

Shiba, Y., Oikonomidis, L., Sawiak, S., Fryer, T.D., Hong, Y.T., Cockcroft, G., Santangelo, A.M., and Roberts, A.C. (2017). Converging prefronto-insula-amygdala pathways in negative emotion regulation in marmoset monkeys. Biol. Psychiatry *82*, 895–903.

Wang, X., Liu, Y., Li, X., Zhang, Z., Yang, H., Zhang, Y., Williams, P.R., Alwahab, N.S.A., Kapur, K., Yu, B., et al. (2017). Deconstruction of corticospinal circuits for goal-directed motor skills. Cell *171*, 440–455.

Wold, S., Ruhe, A., Wold, H., and Dunn, W.J.I.I.I. (1984). The collinearity problem in linear regression. the partial least squares (PLS) approach to generalized inverses. SIAM J. Sci. Statist. Comput. *5*, 735–743.

Xia, L., Nygard, S.K., Sobczak, G.G., Hourguettes, N.J., and Bruchas, M.R. (2017). Dorsal-CA1 hippocampal neuronal ensembles encode nicotine-reward contextual associations. Cell Rep. *19*, 2143–2156.

Yamada, Y., Matsumoto, Y., Okahara, N., and Mikoshiba, K. (2016). Chronic multiscale imaging of neuronal activity in the awake common marmoset. Sci. Rep. *6*, 35722.

Ziv, Y., and Ghosh, K.K. (2015). Miniature microscopes for large-scale imaging of neuronal activity in freely behaving rodents. Curr. Opin. Neurobiol. *32*, 141–147.

STAR★METHODS

KEY RESOURCES TABLE

REAGENT or RESOURCE	SOURCE	IDENTIFIER
Antibodies		
Green Fluorescent Protein (GFP) Antibody	Medical & biological laboratories	MBL598; RRID: AB_591816
Bacterial and Virus Strains		
AAV9-ehSynI-GCaMP7	A.Yamanaka	N/A
AAV2/1-Thy1S-tTA	Sadakane et al., 2015a	N/A
AAV2/1-TRE3-GCaMP6f	Sadakane et al., 2015a	N/A
Chemicals, Peptides, and Recombinant Proteins		
Doxycycline	Sigma Aldrich	D9891
Experimental Models: Organisms/Strains		
Common marmoset (male)	RRD, RIKEN	N/A
Software and Algorithms		
MATLAB	MathWorks	R2016b
nVista HD Software	Inscopix	N/A
Mosaic	Inscopix	1.2
Other		
nVista system	Inscopix	Version 2.0
Prism probe	Inscopix	1050-002203

CONTACT FOR REAGENT AND RESOURCE SHARING

Further information and requests for resources and reagents should be directed to and will be fulfilled by the Lead Contact, Hideyuki Okano (hidokano@a2.keio.jp).

EXPERIMENTAL MODEL AND SUBJECT DETAILS

Three common marmosets (*Callithrix jacchus*; male, body weight: 300–400 g, ages 3–6 years) were used in the present study (identified by letters M, S, and W). All animal experiments were approved by the Animal Research Committee of Keio University School of Medicine (approval number: 11006), and conformed to the National Institutes of Health (1996) guidelines.

METHOD DETAILS

Intracortical microstimulation (ICMS) and adeno-associated virus (AAV) injection

The locations of the forearm primary motor cortex (M1) area were mapped with ICMS as described previously (Kondo et al., 2015). Marmosets were anesthetized by intramuscular (i.m.) injection of ketamine (30 mg/kg) and xylazine (2.5 mg/kg). Body temperature and oxygen saturation levels were monitored. Anesthetized animals were mounted on a custom-made stereotaxic frame (IMPACT-1000B; Muromachi Kikai, Japan) (Figure S1A), and two polyetheretherketone (PEEK) pipes (Muromachi Kikai, Japan) were attached to the skull with dental cement (UNIFAST II, GC, Japan). Two pipes were placed in parallel over the frontal and occipital areas, and both pipes were flanked by small stainless steel bars.

A few days later, the marmosets fitted with head pipes were sedated with an i.m. injection of ketamine (30 mg/kg), atropine sulfate (0.05 mg/kg), ampicillin (50 mg/kg), and dexamethasone (0.30 mg/kg), and sat in a custom-made stereotaxic chair (Muromachi Kikai, Japan). The two pipes were used for head fixation- this allowed us to avoid the use of painful tooth/eye and ear bars. Thus, the marmosets received ICMS under more natural conditions without xylazine treatment (Figure S1B).

A large craniotomy (5 × 5 mm square, without durotomy) was made over the area of the left motor cortex, and tungsten electrodes were implanted to deliver ICMS (10 biphasic pulses composed of 0.2-ms cathodal and 0.2-ms anodal pulses, at 333 Hz). The location of the forearm M1 area was estimated based on the observation of evoked forearm motor responses.

After ICMS, the marmosets were anesthetized using 1%–1.5% isoflurane and an AAV solution was injected into two sites (each site was separated by 1 mm) of the forearm M1 area, 2 mm below the cortical surface. The 500 nL of AAV solution mixture

(AAV2/1-Thy1S-tTA, 2.0 × 10^{11} vg/mL; AAV2/1-TRE3-GCaMP6f, 1.0 × 10^{12} vg/mL) was injected into each site at 100 nL/min through a glass pipette connected to a microinjector (BJ-110; BEX, Japan). After virus injection, the brain surface was washed with saline to reduce the production of connective tissue over the dura. Before skull closure, we took pictures of the blood vessel pattern, ICMS probe trace pattern, and artificial marks made by a rongeur (16621-14; Fine Science Tools, Foster City, CA) (Figure S1C); this allowed us to identify the AAV injection site later. Artificial dura (5 × 5 mm) (PPX-03060; Gore, Japan) was applied to the brain surface, a Kwik-Sil® silicone elastomeric adhesive (World Precision Instruments, Sarasota, FL) was mounted, and the scalp was sutured (Figure S1D).

Lens probe insertion and fixation

A prism probe was implanted into M1 2–3 weeks after AAV injection. Under anesthesia, the scalp was opened and the mounted Kwik-Sil® and artificial dura were removed. After careful removal of connective tissues on the dura, a deep incision (2 mm in depth) was made over the dura along with the line flanked by AAV injection tracks (approximately 1 mm in length) using a sharp surgical blade, and a durotomy was made in a square where one of the sides was incised deeply. Durotomy was performed only at the probe insertion site (~1 × 1 mm); then, to stabilize the inserted probe and reduce brain tissue damage and vessel disruption due to pulsation, the probe was affixed with dental cement (Figure S1E).

The prism probe (1.0 mm in diameter, 4.3 mm in length) (1050-002203; Inscopix, Palo Alto, CA) was attached to the lens implant kit (ProView, 1050-002334; Inscopix, Palo Alto, CA) connected to an endoscope. The edge of the prism was aligned on the incision (Figure S1E) and the prism was inserted until a GCaMP fluorescence signal was detected (~2.3-mm depth). At this position, the probe was fixed to the skull with Metabond® (C&B, Parkell, NY) (Figure S1F). Then the probe top was covered with Kwik-Cast (World Precision Instruments, Sarasota, FL) after the endoscope was disconnected.

An endoscope base plate was attached to the skull using dental cement 3–6 weeks after probe insertion. This varied due to the time needed for recovery from the surgical procedures, and the appearance of clearly defined outlines of cell bodies and vessels (Figure S1G). Each marmoset required an endoscope, base plate, and probe lens for imaging (Figure S1G); the base plate cover remained affixed after imaging (Figure S1H).

AAV production and purification

AAV vectors were produced using the AAV Helper-Free System (Agilent Technologies, Inc., Santa Clara, CA). Detailed methods used for AAV production and purification were described previously (Konishi et al., 2008). pAAV-Thy1s-tTA and pAAV TRE3-GCaMP6f plasmids were used to produce AAV (Sadakane et al., 2015b).

Doxycycline (DOX) treatment

DOX (D9891; Sigma Aldrich, St. Louis, MO) was administered orally using a syringe (2 mg of DOX in 20 mL of 20% honey-syrup solution). To ensure GCaMP expression control by DOX, we checked the GCaMP expression level 3 d after the first administration; an extra 1 mg of DOX was administered as needed. Then, 1 mg of DOX was administered approximately once per month to maintain the desired GCaMP expression levels.

Ladder-climbing task

The ladder apparatus comprised side walls made of clear Plexiglas (1.4 m in height) and wood rungs (4 mm in diameter), with a distance of 4 cm between rungs (Figure S4A). The marmosets were trained to climb the ladder from a carrying cage at the bottom to another carrying cage at the top. Then the carrying cage containing the marmoset was moved to the bottom, and the marmoset began climbing again. To climb up the apparatus (1 session), each hand needed to grip the rungs 5–8 times. The marmosets were pre-trained on the ladder-climbing task before neural recording. Pre-training was performed over 3–5 d (5–10 sessions per day), and testing began when the marmosets climbed up without stopping or turning around.

Lever-pull and pellet retrieval tasks

Each marmoset was trained to wear a custom-made jacket with a Velcro strip, which was used to attach the marmoset to a back plate with a rigid bar (Figure 1D). Each marmoset was habituated for 1–2 weeks so that they would remain calm during the tasks. After successful habituation, the marmosets were trained to perform the following tasks before neural recording.

Lever-pull task: The grip (ball-shaped, 8 mm in diameter) of the lever was located 30 mm in front of the marmoset's right hand (Figure 1D). The animals were pre-trained to pull the lever horizontally. Each marmoset performed the task ~20 times, once per day.

Pellet-reaching task: The pellet (sweet marshmallow, 5 mm in diameter) was placed 30 mm in front and 45° to the right or left side of the home position (Figure 2A). Once a pellet was retrieved, the marmoset needed to wait 3 s, and the next pellet was placed on the other side. Each marmoset performed the task 40 times, once per day.

Data processing

Calcium imaging data were acquired using a miniaturized fluorescence microscope (nVista; Inscopix, Palo Alto, CA) at 20 frames/s. The acquired images were spatially downsampled by a factor of 2 using Mosaic software (Inscopix, Palo Alto, CA). We then performed rigid image registration to correct for lateral brain displacement using the Mosaic software. To normalize the fluorescence

signals to the average fluorescence of the frame, we calculated registered images as percent change (ΔF) over baseline (F): ΔF(t)/F = (F(t) – F)/F. Ca^{2+} transients from individual cells, which predominantly reflect action potentials with a minor contribution from subthreshold potentials (Berger et al., 2007), were identified with established cell-sorting algorithm based on principal component analysis (PCA) and independent component analysis (ICA) (Mukamel et al., 2009). Noted here that PCA-ICA algorithm, as its nature, minimizes signal contaminations from nearby cells or movement-related artifacts (Figure S3). This automated independent component sorting algorithm was used widely in the regions of hippocampus (Xia et al., 2017), sensorimotor cortex (Wang et al., 2017) and other multiple regions in rodents.

QUANTIFICATION AND STATISTICAL ANALYSIS

Detection of spike events from Ca^{2+} transients

For each selected calcium transient trace from a single cell, we subtracted the median trace (20 s sliding window) to minimize negligible fluctuations from baseline. Further, an estimate of the amplitude of fluctuation from baseline was calculated using median absolute deviation (MAD):

$$\mathrm{MAD} = \mathrm{median}_i(\ |X_i - \mathrm{median}_j(X_j)|\ ),$$

where i and j take the values 1, 2, 3..., n_{frames}, and X_i is the intensity of the signal at the i-th frame. MAD is a statistical distribution that is more resilient to outliers in a dataset than the standard deviation. Using the calculated MAD for each trace, calcium events were detected as follows.

First, the algorithm identified the event timing t, where the slope of X_t turns from positive to negative. These positive peaks were classified as candidate Ca^{2+} events. Next, the algorithm identified the most previous event from these positive peaks, where the slope of X_t turns from negative to positive. The MAD value was added to the amplitude of these troughs, and the value was defined as the Ca^{2+} event detection threshold for the subsequent peaks. The positive peaks exceeding this threshold were treated as Ca^{2+} events.

A blinded visual inspection was finally performed to confirm that the detected Ca^{2+} spikes from a single cell were segregated from the signals of neighboring neurons.

Partial least-squares discriminant analysis (PLS-DA)

There are many available statistical tools to model experimental biodata; therefore, a model must be chosen carefully while considering the theoretical assumptions. M1 neurons synchronously fire in milliseconds, and coherently oscillate together at approximately 20 Hz during physical movement. Therefore, it is highly likely that Ca^{2+} dynamics of M1 neurons exhibit multicollinearity. There was no prior knowledge regarding data distribution, as the present study was the first to analyze Ca^{2+} dynamics of M1 neurons in naturally behaving NHPs. Model interpretability is also needed to determine the physiological relevance of the results. Hence, we used PLS-DA to decode movement direction from Ca^{2+} dynamics of M1 neurons during bi-directional arm reaching.

PLS regression combines features of principal component analysis and multiple linear regression, and thereby transforms a set of correlated explanatory variables into a new set of variables that are orthogonal to each other, which is appropriate in the presence of multicollinearity (Wold et al., 1984). PLS is a mathematical estimation approach that builds a model by sequentially adding data points such that model parameters are continuously updated. PLS-DA performs a PLS regression with a dichotomous dependent variable, and is used for classification tasks. PLS-DA is a standard tool in chemometrics, and has been applied to other classification problems in science due to its applicability to multicollinearity and result interpretation (Pérez-Enciso and Tenenhaus, 2003).

Other standard models did not fit the present study, as automated variable selection procedures for logistic regression or linear discriminant analyses generate unstable prediction models in the presence of multicollinearity. When there is no prior knowledge regarding data distribution, the k-nearest neighbors algorithm is useful but is very sensitive to irrelevant variables and multicollinearity because all variables contribute equally to the model. Multilayer perceptron and support vector machine are not severely affected by multicollinearity but model interpretability is very low.

Decoding arm-reaching movement direction using PLS-DA

To predict the arm movement direction $D(i)$ in the i-th trial during bi-directional reaching, the filtered neural Ca^{2+} transient signal data were pooled as the two-dimensional vector, $A_{m,t}(i)$, where m is the neuron ID, and t is time; this describes the neural and temporal information of the i-th trial. The goal of decoding was to estimate a set of weights $\{a_0,\ a_{m,t}\}$ so $D(i)$ could be modeled as their linear combination with $A_{m,t}(i)$

$$D(t) = \begin{cases} 1 & , \text{ if the direction of movement was right} \\ 0 & , \text{ if the direction of movement was left} \end{cases}$$

$$D(t) = a_0 + \sum_m \sum_t a_{m,t} \cdot A_{m,t}(i) + \varepsilon(i) \quad (1)$$

where a_0 is the intercept, $a_{m,t}$ is the weight of the component at that neuron ID and time, and $\varepsilon(i)$ is the residual error at the i-th trial. The optimal number of PLS components for this recoding model was 10, determined by the minimal predictive error sum of squares. For the decoding directions, 23 of 38 trials (Marmoset M), 25 of 41 trials (Marmoset S), and 11 of 18 trials (Marmoset W) were used as training datasets, and the rest were used as test datasets for validation. The decoding was performed 10,000 times repeatedly with different combinations of train-and-test datasets to estimate a proper accuracy rate. The accuracy rate was quantified by determining the percentage of trials in which the actual and predicted directions were the same.

Weights of the prediction model, shown in the following Equation (2), were analyzed to evaluate the contribution of individual neurons to the prediction of movement direction

$$W(m) = \frac{\sum_t a_{m,t}}{\sum_t \sum_m |a_{m,t}|} \quad (2)$$

where $|\bullet|$ represents the absolute value of $\bullet$, and $W(m)$ quantifies the percentage contribution of the m-th neuron for decoding.

Neural order shuffling

To ensure the decoding performance, a shuffling analysis was performed after each decoding model was acquired. For each experiment, surrogate validation datasets were generated, and the decoding model obtained previously from the training data was used to make a prediction on these surrogate validation data. The expected accuracy was 50% in this case. In neural order shuffling, the neuron ID of the validation data was randomly shuffled, while the sample order remained unchanged.

Cell Reports, Volume *24*

Supplemental Information

Calcium Transient Dynamics of Neural Ensembles in the Primary Motor Cortex of Naturally Behaving Monkeys

Takahiro Kondo, Risa Saito, Masaki Otaka, Kimika Yoshino-Saito, Akihiro Yamanaka, Tetsuo Yamamori, Akiya Watakabe, Hiroaki Mizukami, Mark J. Schnitzer, Kenji F. Tanaka, Junichi Ushiba, and Hideyuki Okano

Figure S1

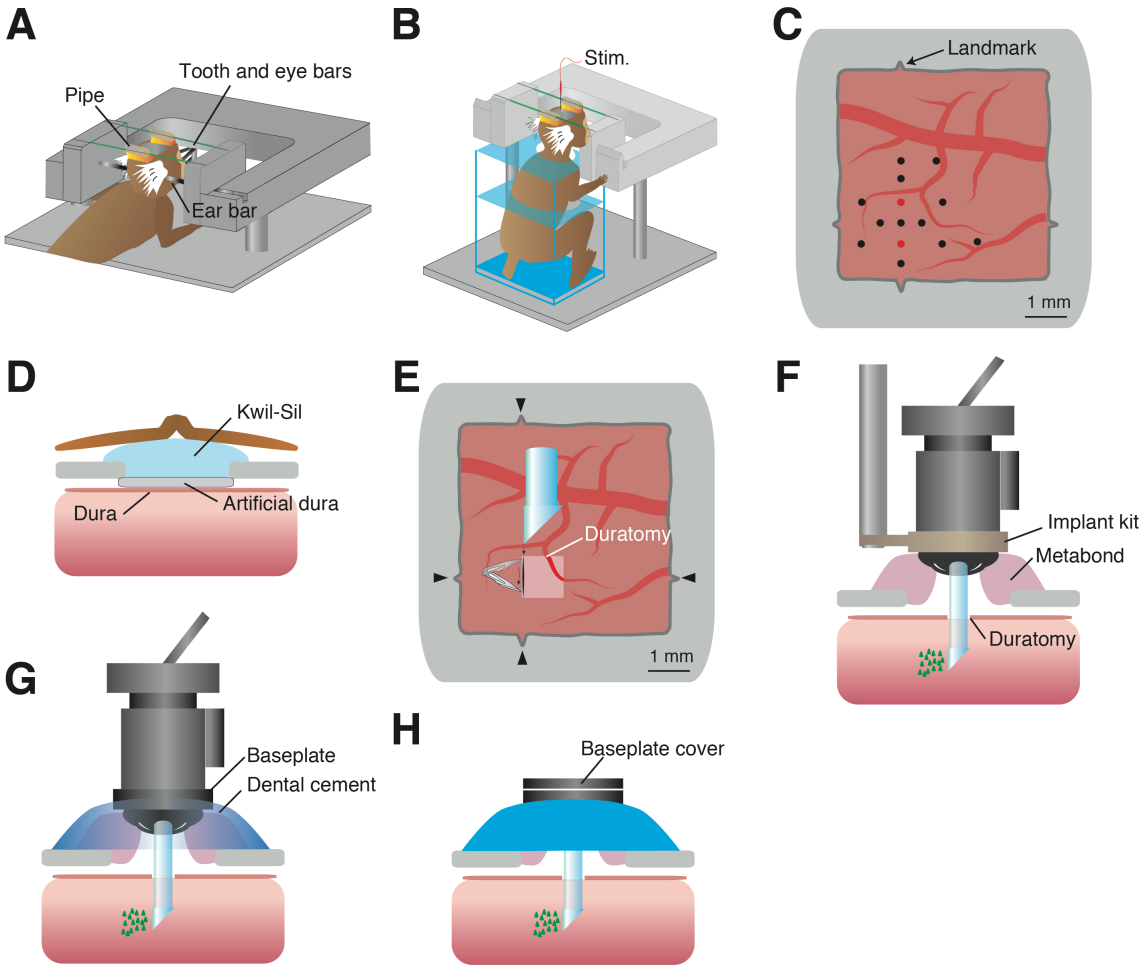

Figure S1. Surgical procedures. Related to Figure 1.

(**A**) Each marmoset was mounted on a custom-made stereotaxic frame with tooth/eye and ear bars (black). Two polyetheretherketone (PEEK) pipes were attached in parallel on the skull.

(**B**) During intracranial microstimulation (ICMS), each marmoset sat in a custom-made chair (blue) and its head was fixed using the pipes.

(**C**) A typical image after ICMS and adeno-associated virus (AAV) injection. Black dots

indicate ICMS sites and red dots are the response sites of the forearm primary motor cortex (M1). AAV was injected into the locations indicated by the two red dots. Before scalp closure, artificial landmarks (bone cracks, black triangles) were made to help subsequently identify the AAV injection sites.

(**D**) Treatment while waiting for GCaMP expression. Artificial dura was placed over the dura, Kwik-Sil® was applied, and the scalp was sutured.

(**E**) Durotomy. A deep incision (2 mm in depth) was made between the two AAV injection sites, and a square durotomy was performed (approximately 1 × 1 mm).

(**F**) Prism probe insertion. The probe was attached to the implant kit with an endoscope, and the edge of the probe was aligned to the incision. The probe was inserted until a GCaMP fluorescence signal was detected, then the probe was fixed to the skull with Metabond®.

(**G**) Base plate mounting. Three to 6 weeks after probe insertion, a base plate with an endoscope was fixed to the skull using dental cement. Ca^{2+} imaging was accomplished using this setup.

(**H**) The endoscope was removed and the base plate cover was attached to the base plate when the marmoset was not actively engaged in imaging experiments.

Figure S2

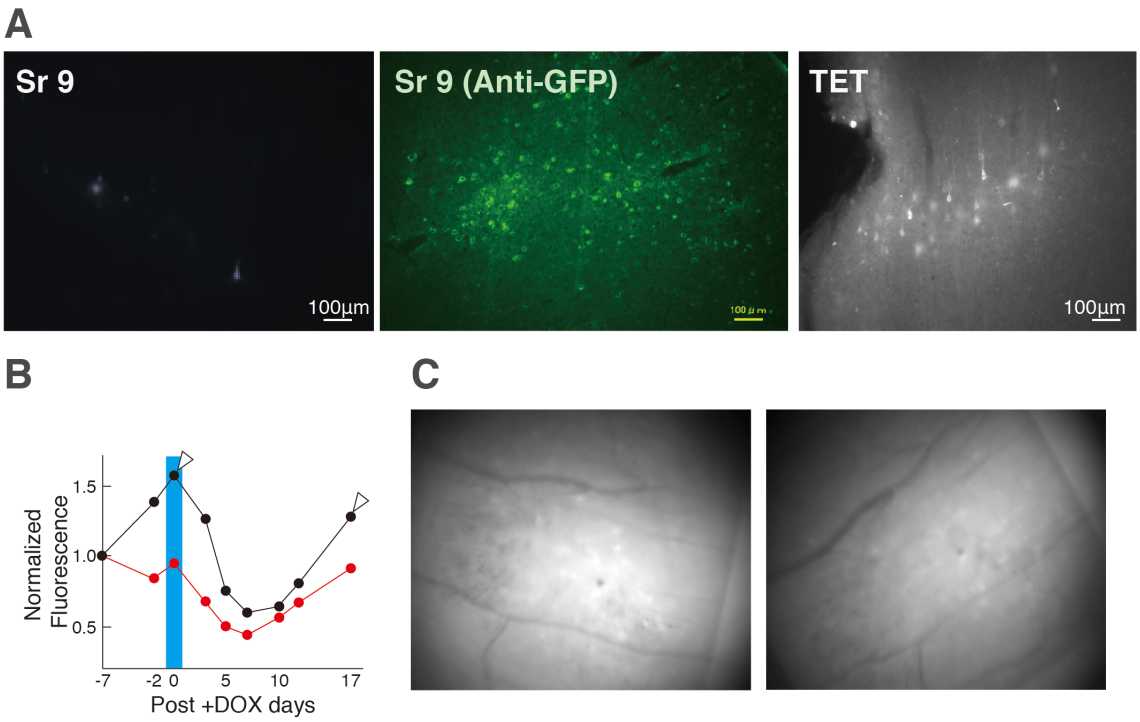

Figure S2. Strong and controllable GCaMP expression by AAV vectors using the tetracycline-controlled transcriptional activation (Tet)-Off system. Related to Figure 1.

(**A**) After careful selection of an AAV serotype compatible with marmoset neurons, we decided to use Serotype 9, as it produced the strongest gene induction (data not shown). However, an enhanced human synapsin promoter-GCaMP7 simple construct (AAV9-ehSynI-GCaMP7) failed to induce GCaMP sufficiently enough to visualize transfected cells with an endoscope (left: direct fluorescence, 7 weeks after AAV injection; middle: indirect fluorescence with a green fluorescent protein [GFP] antibody). Tet-system-mediated

GCaMP expression was strong enough to be detected using direct fluorescence (right).

(**B**) Doxycycline (DOX) treatment excessively reduced GCaMP expression. The time course of the averaged direct fluorescence intensity before and after DOX administration.

Tet-system-mediated GCaMP6f expression was downregulated by a single administration of 2 mg of DOX. These images were taken from Marmosets W (black) and M (red). The exposure time and light intensity were the same. We conducted Ca^{2+} imaging 5–10 d after a single DOX administration.

(**C**) Images of primary motor cortex (M1) neurons on Day 0 and Day 17 after DOX administration in Marmoset W (also see arrowheads in b). Downregulation of GCaMP expression was recovered 3 weeks later. A single DOX administration, similar to that used previously, was necessary to repeat the Ca^{2+} imaging.

Figure S3

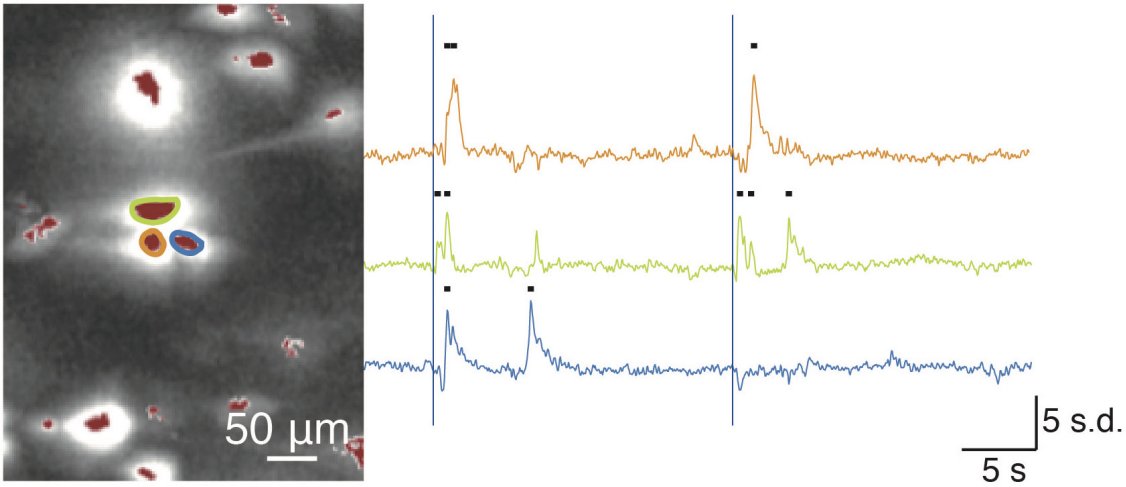

Figure S3: Images of neurons located nearby in a single field of view with their region of interest (ROI) spatial filters. Related to Figure 1.

Time traces for three of these cells (highlighted with brightly colored outlines are shown. The florescent signals of each cells changed independently. The vertical lines indicate the onset of lever pulling in Figure 1F.

Figure S4

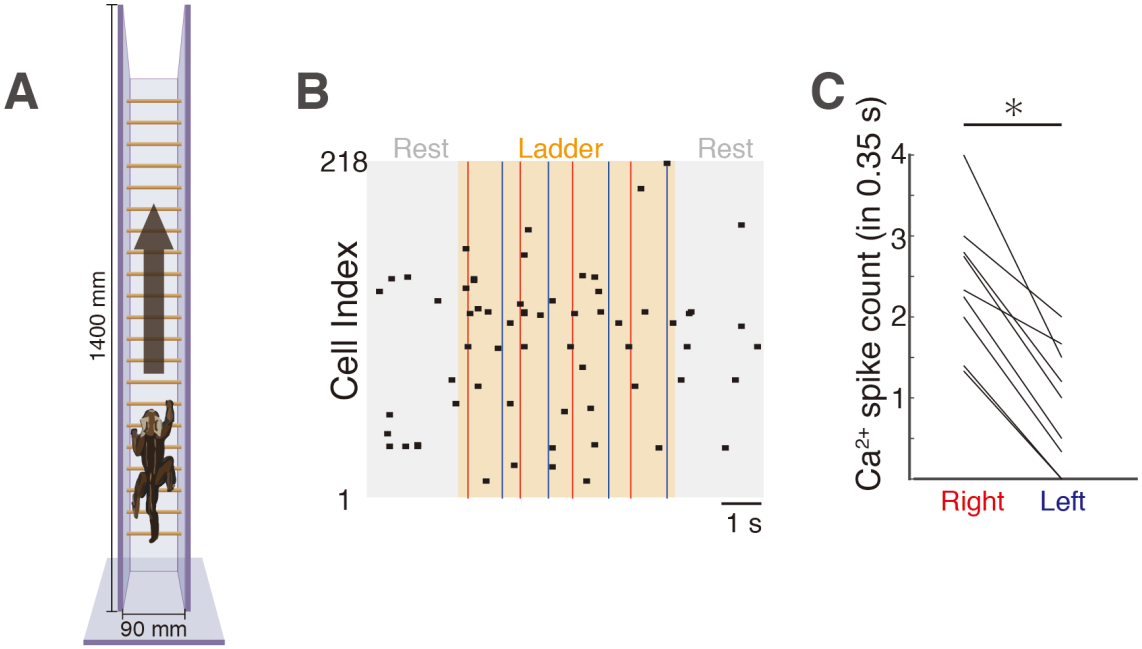

Figure S4. Neural recordings during the ladder-climbing task, a natural movement pattern. Related to Figure 1.

(**A**) The ladder apparatus consisted of Plexiglas walls (1.4 m in height) and wood rungs (4 mm in diameter); the distance between rungs was 40 mm.

(**B**) A raster plot of the Ca^{2+} events recorded during the ladder-climbing task. The vertical lines indicate the time at which each forearm reached the rung (red: right forearm; blue: left forearm). The frequency of the Ca^{2+} events increased with each rung.

(**C**) Across nine sessions, Ca^{2+} event count increased when the right forearm reached for the rung compared with the left forearm (Ca^{2+} spikes were counted in 0.35 s around the time when

the paw touched the rung, averaged from 218 neurons; paired t-test, $p < 0.05$).

Figure S5

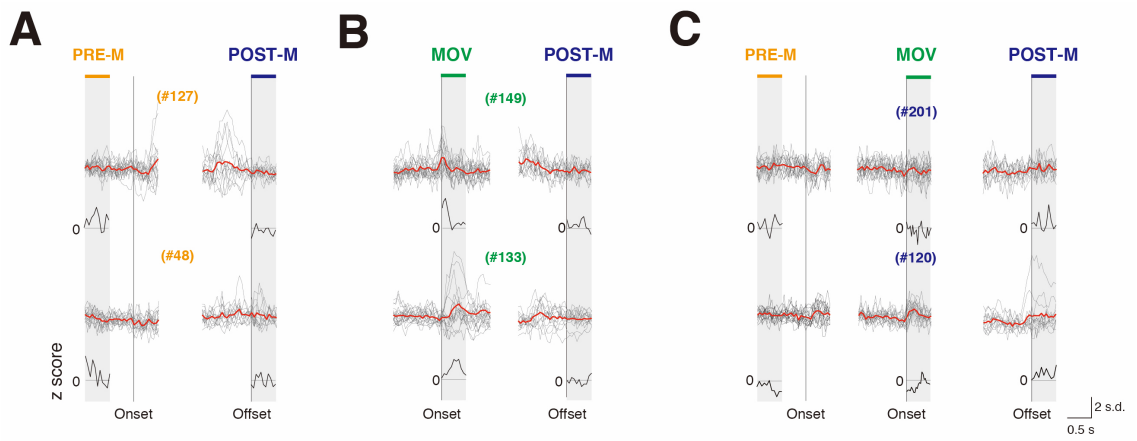

Figure S5. Reaching-direction-sensitive neurons during reaching offset (POST-M) did not participate in neural decoding during reaching onset (PRE-M) or during reaching (MOV). Related to Figure 2.

Representative Ca^{2+} transient signals of neurons contributing to movement-direction decoding.

(**A**) Neurons #127 and #48 showed movement-direction-sensitive Ca^{2+} event during PRE-M, but no contribution to decoding was made during POST-M.

(**B**) Neurons #149 and #133 showed movement-direction-sensitive Ca^{2+} event during MOV, but no contribution to decoding was made during POST-M.

(**C**) Neurons #201 and #120 showed movement-direction-sensitive Ca^{2+} event during POST-M, but no contribution to decoding was made during PRE-M or MOV.

Table S1

Table S1. Neurons contributing to neural decoding during reaching onset (PRE-M), reaching (MOV), and reaching offset (POST-M), respectively. The number and percentage indicate the proportion of movement-direction-sensitive neurons in the identified neurons. A checked box denotes the presence of cells in that period. Related to Figure 2.

Marmoset M

PRE-M	MOV	POST-M	Number (%)
✔	×	×	7 (3.42)
✔	✔	×	0
✔	×	✔	0
✔	✔	✔	0
×	✔	×	19 (9.27)
×	✔	✔	1 (0.05)
×	×	✔	7 (3.42)

Marmoset S

PRE-M	MOV	POST-M	Number (%)
✔	×	×	3 (3.37)
✔	✔	×	0
✔	×	✔	0
✔	✔	✔	0
×	✔	×	3 (3.37)
×	✔	✔	0
×	×	✔	3(3.37))

Marmoset W

PRE-M	MOV	POST-M	Number (%)
✔	×	×	2 (1.87)
✔	✔	×	0
✔	×	✔	0
✔	✔	✔	0
×	✔	×	4 (3.74)
×	✔	✔	0
×	×	✔	3 (2.80)